energies

MDPI

Article

Performance Assessment of an Air-Type BIPVT Collector with Perforated Baffles through Indoor and Outdoor Experiments

Jin-Hee Kim [1], Ji-Suk Yu [2], Erin Gaucher-Loksts [3], Benjamin Roy [3], Véronique Delisle [3] and Jun-Tae Kim [2,*]

[1] Green Energy Technology Research Center, Kongju National University, Cheonan 31080, Korea; jiny@kongju.ac.kr
[2] Department of Energy Systems Engineering, Graduate School of Energy Systems Engineering, Kongju National University, Cheonan 31080, Korea; sook1991@smail.kongju.ac.kr
[3] CanmetENERGY, Natural Resources Canada, 1615 Lionel-Boulet Blvd, Varennes, QC J3X 1P7, Canada; erin.gaucher-loksts@nrcan-rncan.gc.ca (E.G.-L.); benjamin.roy@nrcan-rncan.gc.ca (B.R.); veronique.delisle@nrcan-rncan.gc.ca (V.D.)
* Correspondence: jtkim@kongju.ac.kr; Tel.: +82-41-521-9333

Abstract: The performance of air-type PVT and BIPVT collectors has been extensively studied. As a system that generates heat and power, PVT collector testing has some particularities especially when using air as a heat recovery fluid and a building-integrated design (BIPVT). The electrical and thermal experimental performance of such collectors are currently being evaluated using in-house methods or PV and/or solar thermal collector standards. The use of a wide range of methods, testing conditions and experimental setups makes it difficult not only to compare the performance of different designs, but also to have confidence in the results obtained. This study evaluates the performance of an air-type BIPVT collector with in-channel perforated baffle plates for heat transfer enhancement designed for a building-integrated façade. As part of a joint research project between Korea and Canada, the proposed collector's performance was evaluated through indoor (Canada) and outdoor experiments (Korea). Limited comparison of the results obtained with the two testing methods could be performed due to differences in environmental testing conditions, BIPVT collector area and experimental setup. Nevertheless, the limited measurement points under comparable testing conditions indicate that the results from the indoor and outdoor experiments have a similar trend. A comparison between the studied collector having a full PV absorber and a BIPVT collector with a hybrid PV/solar thermal collector absorber using a similar indoor experimental setup and testing conditions was performed. It showed that under still air conditions, for an irradiance level of approximately 820 W/m^2 and with a low flow rate, the BIPVT collector with a hybrid PV/solar thermal absorber has a thermal and electrical efficiency of 25.1% and 5.9%, respectively. Under similar conditions, the BIPVT collector with a full PV absorber has a thermal efficiency of 23.9% and an electrical efficiency of 13.5%. At higher flowrates, both units have similar thermal efficiencies, however, the BIPVT collector with a PV absorber remains with an electrical efficiency that is more than double that of the unit with a hybrid PV/solar thermal absorber.

Keywords: air-type BIPVT (building-integrated photovoltaic with thermal recovery); electrical and thermal performance; performance assessment; indoor and outdoor experiments

Citation: Kim, J.-H.; Yu, J.-S.; Gaucher-Loksts, E.; Roy, B.; Delisle, V.; Kim, J.-T. Performance Assessment of an Air-Type BIPVT Collector with Perforated Baffles through Indoor and Outdoor Experiments. *Energies* **2022**, *15*, 3779. https://doi.org/10.3390/en15103779

Academic Editor: Ahmed Amine Hachicha

Received: 18 April 2022
Accepted: 17 May 2022
Published: 20 May 2022

1. Introduction

In recent decades, efforts have been made to lower energy consumption worldwide towards reducing the effects of climate change and carbon emissions [1]. According to a report by the UN Environment program in 2020, the building sector accounted for 35% of global energy consumption and related 38% of carbon emissions [2]. Therefore, it is necessary to reduce energy use and carbon emissions in the building sector. To this end, the International Energy Agency (IEA) believes that renewable energy systems and energy efficiency measures are key to economic growth by strengthening national

energy policies and reducing carbon emissions. In addition, among renewable energy sources, solar energy systems have achieved remarkable growth over the past 10 years as it can be applied most efficiently into buildings [3]. When integrated into buildings, solar energy systems can cut down heating and lighting loads, and the electricity or thermal energy produced by solar energy systems has the advantage of reducing the building's dependence on grid electricity for heating and cooling. Photovoltaic systems (PV), which have recently been increasing in distribution among solar energy systems, are applied in the form of attachment or integration to buildings. However, there is a problem in that the temperature of the PV module increases during conversion of sunlight into electrical energy. The increasing PV temperature consequently decreases the efficiency of electrical power generation. To solve this challenge, recent studies have focused on lowering the PV module temperature by applying materials such as aluminum heat sink, phase change material and aluminum fins, aluminum fins and ultrasonic humidifier to the rear of the PV module. As a result, PV module temperature reduced by 10–14 °C, while electric efficiency increased by 4–6.8% [4–6]. Concerning heat transfer, air-type PVT collector uses air as the heat transfer medium and produces electricity and heat source at the same time. Air also passes through the back of the PV module, which lowers the module's temperature. The PVT collector is easy to construct in connection with heating and cooling equipment. Besides, a distinctive advantage is that the energy produced can be used directly in equipment such as air handling units, heat recovery ventilators, air conditioners, etc.

Contrary to standard PV modules and solar thermal collectors, air-type photovoltaic collectors with thermal energy recovery (PVT) can simultaneously produce heat and electricity. This brings a number of additional challenges when it comes to performance characterization. This section provides an overview of different testing methods, conditions and experimental setups used to evaluate the performance of PVT and building-integrated PVT collectors (BIPVT).

Zondag et al. [7] and De Vries [8] performed outdoor tests to validate a PVT numerical model. They controlled the inlet temperature and measured the outdoor temperature, irradiance and wind speed. Adeli et al. [9] optimized the thermal and electrical efficiency of air-based PVT collectors with an outdoor experiment. They measured irradiance, ambient temperature, inlet/outlet temperature, PV cell temperature, inlet air velocity, wind speed, open-circuit voltage (V_{oc}) and short-circuit current (I_{sc}) as well as current (I_{mp}) and voltage (V_{mp}) at maximum power point. The inlet air velocity was kept constant on a clear day, and the experiments were performed with varying irradiance and wind speed. The results showed an increase in thermal efficiency from 46.5% to 49% and electrical efficiency from 5.5% to 7.5%. Rahim et al. [10] performed outdoor experiments comparing PV and PVT systems. The PVT inlet air flow was kept at 25 LPM and 50 LPM (1.8 and 3.6 kg/h). Throughout the experiment, the solar radiation, outside temperature, and inlet fluid temperature varied from 600 to 1200 W/m^2, 30 to 40 °C and 35 to 40 °C, respectively. Tomar et al. [11] conducted outdoor tests in New Delhi with four PVT configurations (1) Glass-to-Glass, (2) Glass-to-Backsheet, (3) with a duct and (4) without a duct. During the tests, solar radiation ranged between 300 and 900 W/m^2 and the flow rate was maintained at 0.0058 kg/s (20.88 kg/h). The outside air and inlet fluid temperatures were kept between 25 and 35 °C in the summer and 8 and 23 °C in the winter. They found that the Glass-to-Glass PVT collector had higher thermal and electrical efficiencies. Ozakin et al. [12] performed experiments with different materials and fin configurations in an air-type PVT collector channel. They analyzed electrical, thermal and exergy efficiencies to determine the combination of control parameters that had the most effect on collector performance. Considering constant average ambient, PV module and operating temperatures, the experiments were carried out with an airflow rate varying between 0.05 and 0.065 kg/s (180 to 234 kg/h). The results indicated that the fin material, airflow and PV module temperature had the highest effect on the performance. Ciftci et al. [13] analyzed the performance of an air-type PVT dryer with and without fins. The environmental conditions were 791–827 W/m^2 for irradiance and 27–28 °C for outdoor temperature. The collector thermal efficiency was

found to be between 47.5% and 54.9% without fins and 50.3% and 58.2% with fins for an airflow rate varying between 0.010 and 0.014 kg/s (36 and 50 kg/h). Mojumder et al. [14] proposed an air-type PVT system with thin rectangular fins to promote heat dissipation. The collector performance was analyzed as a function of the number of thin flat metallic sheets used. An indoor experiment was conducted with a solar simulator. The measurements included the PV module's front/back surface and air inlet/outlet temperatures. The mass flow rate and irradiance ranged from 0.02 to 0.14 kg/s (72 to 504 kg/h) and 200 to 700 W/m^2, respectively. The PVT collector thermal efficiency rose from 38% to 56% with increasing number of fins and improved with irradiance and mass flow rate.

Yang et al. [15] experimentally examined and compared the thermal characteristics of a one- and two-inlet BIPVT system under varying irradiance, wind speed and ambient temperature conditions. The experiments were performed in accordance with EN 12975:2006 and ISO 9806-1:1994 using a solar simulator. Various temperature measurements were performed including the back surface of the PV modules, the inner surface of the back insulation layer and within the air channel. Tests were performed at air flow rates of 55, 123, 250 and 370 kg/h. Results showed that the two-inlet BIPVT system increased the thermal efficiency by 5% compared to the one-inlet system.

Cremers et al. [16] conducted an outdoor experiment to evaluate the performance of two PVT collectors with and without backside shielding at set inlet temperatures of 15 and 7 °C. The thermal performance was assessed in accordance with ISO 9806:2013, and measurements were taken for flow rate, inlet/outlet temperature, wind direction/speed, irradiance, scattered radiation, pressure, ambient temperature and relative humidity. The PV module operated in open-circuit and the tests were performed in quasi-dynamic state. The results were analyzed under an irradiance of 800 W/m^2, ambient temperature of 20 °C and wind speeds of 1, 2 and 3 m/s. Results showed that shielding improved the collector efficiency by 20% to 30%

Dittmann et al. [17] performed indoor and outdoor experiments on an unglazed PVT collector. The outdoor experiments aimed at validating indoor measurements and examining the collector behaviour under actual operating conditions. During the tests, the PV module operated in Maximum Power Point Tracking (MPPT) mode. The electrical performance was evaluated under three conditions (1) IEC 61215 at Standard Testing Conditions (STC), (2) fixed external temperature and varying fluid temperature, (3) fixed fluid temperature and varying external temperature. The thermal performance evaluation was based on EN 12975 and ISO 9806. As a result, the PVT collector was found to have similar temperature coefficients in both indoor and outdoor testing conditions.

Bahtiar et al. [18] conducted indoor and outdoor tests with an air-type PVT collector for an exergy analysis. The results were compared at an irradiance of 820 W/m^2, and a mass flow rate varying between 0.01 and 0.05 kg/s (36 kg/h and 180 kg/h). The difference in the calculation of the PVT exergy efficiency using the measurements from the indoor and outdoor tests was found to be in the order of 2%.

This review shows that researchers have been performing air-based PVT and BIPVT collector testing and evaluating their thermal and electrical performance using a variety of methods. Some of these methodologies are based on actual solar thermal collector standards (ISO 9806, EN 12975) or PV module standards (IEC 61215) (or a combination of both). Other methodologies have been developed in-house for the specific purpose of the experiment. The use of a wide range of methods, testing conditions (flowrate, inlet fluid temperature, PV operation mode, wind speed, irradiance, etc.) and experimental setups, as shown in Table 1, makes it difficult not only to compare the performance of different designs, but also to have confidence in the results obtained. As such, the results presented in literature cannot be compared with the different designs utilized in this study.

Table 1. Literature review summary.

Reference	Design Type	Collector Area Tested	Standards Used	Experimental Conditions	Performance (~800 Wm^2 and 2.5 m/s Wind)
Adeli et al. [9]	PVT air collector	0.46 m^2	-	Odoor tests $G = 400–810$ W/m^2 $T_a = 30–36$ °C $V_w = 0–1.2$ m/s	$\eta_{pv} = 9\%$, $\eta_{th} = 37\%$ at $G = 800$ W/m^2, $T_a = 36$ °C, $V_w = 1.2$ m/s
Tomar et al. [11]	GtoG PV and GtoT PV module with air space	0.69 m^2	-	Outdoor tests $G = 200–900$ W/m^2 $T_a = 23–35$ °C	$\eta_{pv} = 11.5–13\%$, $\eta_{th} = 40\%$
Ciftci et al. [13]	PVT system with fins	-	-	Outdoor tests $G = 700–900$ W/m^2 $T_a = 24–30$ °C $\dot{m} = 0.01–0.014$ kg/s	$\eta_{th} = 70\%$ at $G = 900$ W/m^2, $T_a = 30$ °C, $\dot{m} = 0.014$ kg/s
Mojumder et al. [14]	Air type PVT collector with cooling fins	0.31 m^2	ISO 9806:1994	Outdoor tests $G = 200–700$ W/m^2 $T_a = 25$ °C $\dot{m} = 0.02–0.14$ kg/s	$\eta_{pv} = 14.0\%$, $\eta_{th} = 56.2\%$ at $G = 700$ W/m^2, $\dot{m} = 0.14$ kg/s
Yang et al. [15]	Two-inlet air based BIPVT	1.07 m^2	-	Indoor tests $G = 1040$ W/m^2 $T_a = 20$ °C $V_w = 2.1–3.1$ m/s	$\eta_{th} = 50\%$ at $\dot{m} = 370$ kg/h, $V_w = 2.1$ m/s
Cremers et al. [16]	1. Laminated glass-PV-absorber module (serpintine copper tubes) with a air gap of 66 mm^2. Laminated glass-PV-glass with holohedral polypropylene absorber with ann air gap of 80 mm	1. 3.8 m^2 2. 4.4 m^2	ISO 9806:2013	Outdoor tests 3 days $G = 800$ W/m^2 $V_w = 1–3$ m/s $T_a = 7–15$ °C	$\eta_{th} = 20\%$ at $G = 800$ W/m^2, $V_w = 2$ m/s, $T_a = 20$ °C and at stagnation and open circuit mode
S. Dittmann et al. [17]	Commercial unglazed PVT collector with a heat exchanger plate on its back side	1.64 m^2	Electrical characterization:IEC 61215:2005 Thermal characterization: EN12975/ISO9806	Electrical characterization: Indoor tests $G = 1000$ W/m^2 $T_a = 25–60$ °C $T_f = 5–75$ °C Thermal characterization: Outdoor/indoor tests $V_w = 0–3$ m/s $T_m^* = 0–0.05$ $\frac{°C \cdot m^2}{W}$	$\eta_{pv} = 14.4\%$ at STC $\eta_{th} = 28\%$ at $T_m^* = 0.02$ $\frac{°C \cdot m^2}{W}$, $V_w = 1.5$ m/s and is at MPP
Bathtiar et al. [18]	PVT system solar air collector	-	-	Outdoor tests $G = 820$ W/m^2 $T_a = 25$ °C $\dot{m} = 0.02$ kg/s	$\eta_{pv} = 10.3\%$, $\eta_{th} = 51.9\%$ at indoor test $\eta_{el} = 10.5\%$, $\eta_{th} = 50.3\%$ at outdoor test

The main objectives of this paper are to:

- Demonstrate how existing PV and solar thermal standards can be used for thermal and electrical characterization of BIPVT units.
- Compare the results obtained with indoor and outdoor performance characterization experiments of an air-based BIPVT unit and highlight the challenges of doing such comparison.
- Compare the performance of an air-type BIPVT collector with in-channel perforated baffle plates with that of a BIPVT unit with a hybrid PV/solar thermal collector absorber to demonstrate the thermal and electrical impact of such design.

In order to achieve these objectives, an air-type BIPVT collector with in-channel perforated baffle plates was tested in both indoor (Canada) and outdoor (Korea) conditions based on the thermal performance evaluation standard (ISO 9806 [19,20]) and the electrical performance evaluation standard (IEC 60891 [21]). The BIPVT collector indoor performance characterization was done with two different experimental setups to evaluate the electrical and thermal performance under varying levels of irradiance and ambient temperature (electrical) as well as flowrate, irradiance, inlet air temperature and wind speed (thermal). The outdoor experiment analyzed the electrical and thermal performance under steady-state conditions at different irradiance levels, flowrates and inlet temperatures.

2. Air-Type BIPVT Collector

The proposed air-type BIPVT collector is comprised of a Glass-to-Backsheet (G-to-B) type PV absorber, air channel and insulation (Figure 1), as described in [22]. The uniquely designed BIPVT collector utilizes the perforated thermal plate, located in the BIPVT collector cavity to enhance heat transfer performance. Two identically designed

modules with different areas, modules 1 and 2, are utilized for the indoor and outdoor experiments, respectively. The characteristics of each module are listed in Table 2.

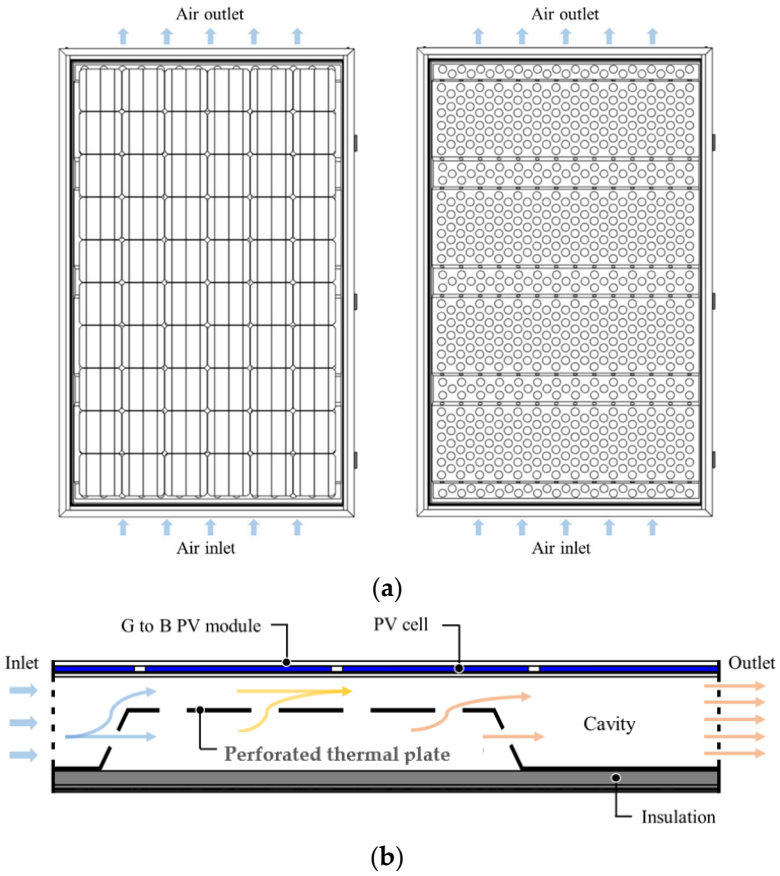

Figure 1. Air-type BIPVT collector schematic: (**a**) Top view module (**left**) and perforated thermal plate (**right**) and (**b**) cross-sectional profile showing airflow direction.

Table 2. Key characteristics of modules 1 and 2 provided by the manufacturer.

Parameter	Module 1 (Indoor)	Module 2 (Outdoor)
Cell type	Monocrystalline silicon	Monocrystalline silicon
Gross length	1.68 m	1.90 m
Gross width	1.04 m	1.11 m
Number of cells	60	66
Depth	6 mm	6 mm
PV power at maximum power point (P_{mp})	286 W	308 W
Voltage at maximum power point (V_{mp})	33.9 V	33.0 V
Current at maximum power point (I_{mp})	8.4 A	9.3 A
Open-circuit voltage (V_{oc})	41.1 V	44.5 V
Short-circuit current (I_{sc})	9.0 A	9.7 A
Electrical efficiency at maximum power point (η_{pv})	17.0%	14.6%

3. Experimental Setup

Three experimental analyses were completed utilizing the BIPVT modules described in Section 2: indoor electrical, indoor thermal and outdoor characterizations.

The indoor performance characterization of the BIPVT module was done with two different experimental setups to obtain the electrical and thermal characterization under

steady-state conditions. The first indoor performance test provides the electrical characteristics under different conditions of irradiance level and module temperature. The second indoor characterization test evaluates the thermal performance under steady-state conditions at different flowrates, irradiance levels, wind speeds and inlet air temperatures.

The outdoor performance characterization of the BIPVT module was conducted in a closed-loop configuration to obtain both the electrical and thermal characteristics at observed steady-state conditions.

It is important to note that both the indoor and outdoor experimental analysis used a similar methodology as an ordinary PVT collector. Therefore, the BIPVT collector performance could differ when integrated into a building.

3.1. Indoor Electrical Characterization

The indoor test was completed in a Large Area Pulse Solar Simulator (LAPSS) (see Figure 2). The solar simulator is rated class A+ for spectral match, irradiance uniformity and long and short-term pulse stability according to IEC 60904-9 [23]. The simulator includes an I-V curve tracer to measure current-voltage (I-V) characteristics. The temperature of the units under test can be regulated between 15 and 75 °C with a temperature homogeneity of 0.5 °C. As for the irradiance, it can be varied between 200 and 1100 W/m^2 with a flash duration of up to 110 ms.

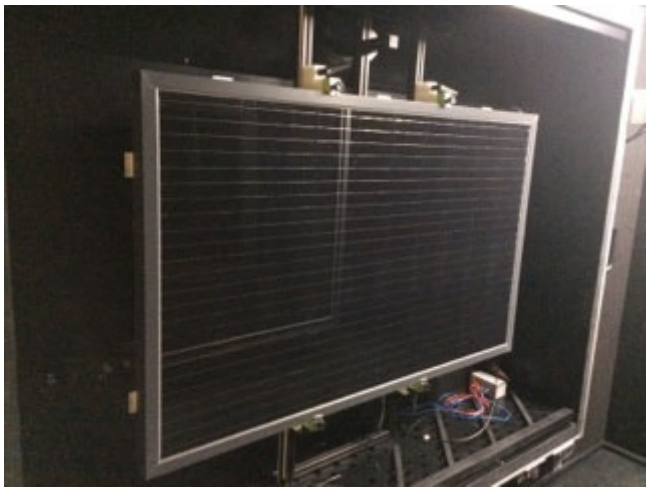

Figure 2. BIPVT module installed in the LAPSS.

I-V curves of the BIPVT units were obtained at four values of PV module temperature T_{pv} (15, 25, 50 and 75 °C) and irradiance levels G (200, 500, 800, 1000 W/m^2). The module temperature during testing was obtained by averaging measurements taken by three sensors attached at the back surface of the module. I-V curves were taken when all three sensors had reached thermal steady-state, i.e., when they were at a uniform temperature.

3.2. Indoor Thermal Characterization

The indoor testing was completed at the Concordia University Paul Fazio Solar Simulator and Environmental Chamber (SSEC) located in Montreal, Canada. As shown in Figure 3, the simulator consists of a set of eight metal halide lamps (ATLAS MTT Solar Constant 4000-watts lamps) with adjustable location and intensity that emulates a solar spectrum corresponding to an air mass of 1.5. An artificial sky located between the lamps and the testing rig minimizes the impact of long-wave irradiance measured by a pyrgeometer. The testing rig used to mount the units under test has a wind generator located at the bottom. A pyranometer and hot-wire anemometer, mounted on a mobile scanning unit, measure the distribution and uniformity of irradiance level and wind speed across the collector, respectively. A distribution box is used at the outlet as an adapter to promote airflow uniformity inside the collector.

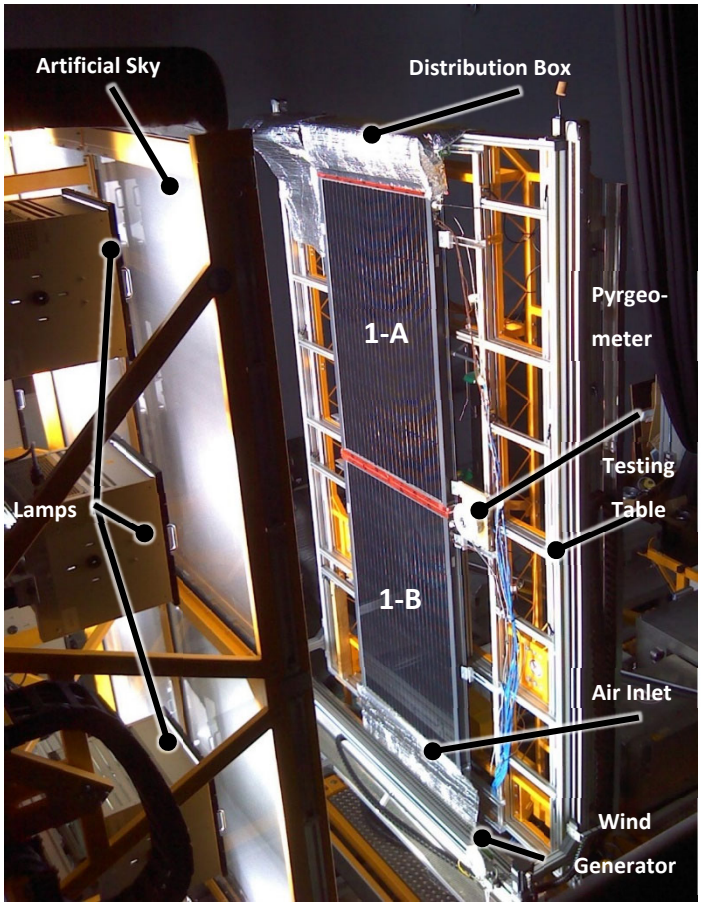

Figure 3. Components of the SSEC.

Two modules were installed in series and tested under two different configurations: open- and closed-loop. The open-loop test evaluates the collector performance dependence to wind speed, irradiance and airflow rate at a constant inlet air temperature corresponding to ambient. The closed-loop test characterizes the collector performance dependence to the reduced temperature difference at a constant wind speed, irradiance and airflow rate. Both configurations require the modules to be connected to an air testing loop located downstream, comprised of a variable-speed blower, an air flowmeter measuring station and a pressure sensor as well as an Archimedean spiral RTD temperature sensor that measures the average air temperature according to ISO 9806:2017 [20]. All instruments used and their accuracy are listed in Table 3. In open-loop configuration, the modules are mounted vertically and ambient air is circulated in the collector, as seen in Figure 4. The inlet air temperature is measured by three thermocouples located at the inlet of module 1-B. In the closed-loop configuration, the modules are tested horizontally due to space limitations. An electrical heater located upstream of the collector raises the inlet temperature above ambient. Another distribution box at the collector inlet connects the heating system to the BIPVT units, as seen in Figure 5. For both configurations, the average PV cell temperature for both modules is measured by 22 thermocouples mounted at the back surface of the absorber rear glass sheet.

Table 3. Instrument specifications.

Measurement	Instrument Type	Instrument Accuracy
Ambient temperature T_a	RTD Class A	$0.15\ ^{\circ}\text{C} + 0.2\% \cdot T_a$
Outlet temperature T_o	RTD Class B	$0.30\ ^{\circ}\text{C} + 0.5\% \cdot T_o$
Inlet temperature open-loop T_i	Thermocouple Type T	$0.5\ ^{\circ}\text{C}$
Inlet temperature closed-loop T_i	RTD Class B	$0.30\ ^{\circ}\text{C} + 0.5\% \cdot T_i$
Ambient relative humidity RH	–	1% RH
Ambient pressure p_a	Manometer	$0.8\% \cdot p_a$
Air flowrate $\dot{m}$	Orifice plate flowmeter	$2\% \cdot \dot{m}$
Wind speed V_w	Hot-wire anemometer	$0.1\ \text{m/s} + 0.02 \cdot V_w$
Irradiance G	Pyranometer	$3.2\% \cdot G$
PV cell temperature T_{pv}	Thermocouple Type T	$0.5\ ^{\circ}\text{C}$
Net long-wave irradiance E_L	Pyrgeometer	$5\ \frac{\text{W}}{\text{m}^2}$
Current I	I-V curve tracer	$\max(0.5\% \cdot I; 45\ \text{mA})$
Voltage V	I-V curve tracer	$\max(0.5\% \cdot V; 28\ \text{mV})$

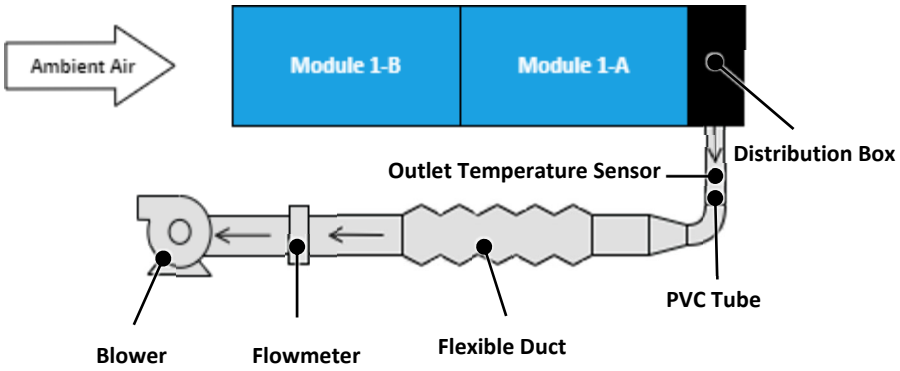

Figure 4. Open-loop schematic at the SSEC.

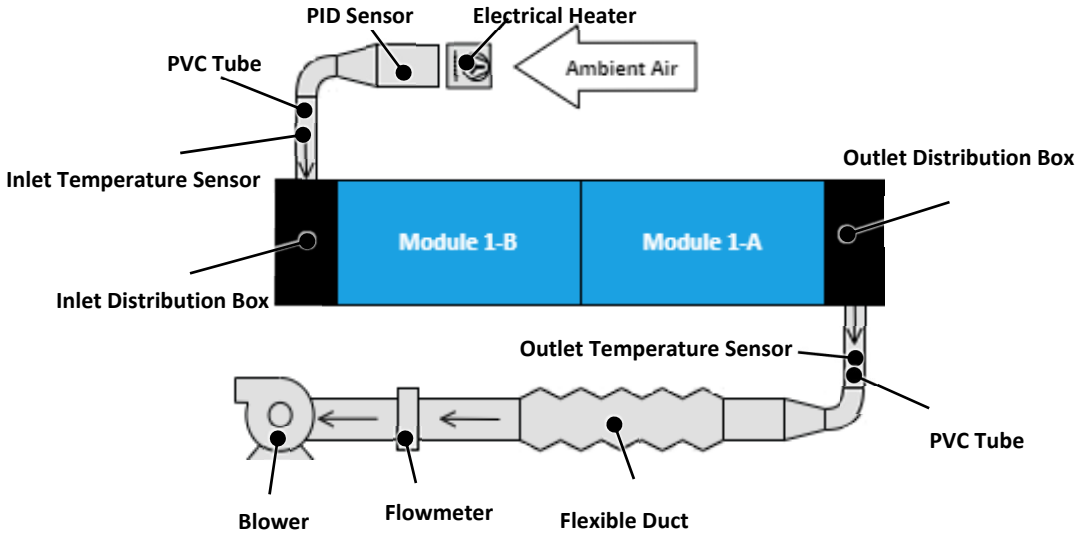

Figure 5. Closed-loop schematic at the SSEC.

Ambient conditions are controlled with the room air-conditioning system. During testing, the ambient air temperature T_a varied between 22 °C and 26 °C and the air relative humidity RH between 19% and 31%. The test conditions for the steady-state performance characterization are summarized in Table 4.

Table 4. Test conditions for the indoor steady-state performance characterization.

$\dot{m}_o$ kg/h	G (W/m^2)	Open-Loop			Closed-Loop		
		V_w			T_i		
		Still Air [1]	2.4 m/s	4.6 m/s	35 °C	45 °C	55 °C
85	821	x o	x	x	o	o	o
	939	x	x	x			
	1060	x	x	x			
195	821	x	x	x		o	
	939	x	x	x			
	1060	x	x	x			
350	821	x	x	x			
	939	x	x	x			
	1060	x	x	x			

x: Tested in vertical position. o: Tested in horizontal position. [1] Wind generator is off, slight air circulation in the room occurred due to the ventilation system of the building.

The irradiance spatial non-uniformity was found to be at most 9.2%. This is better than the 15% non-uniformity required by the solar thermal collector testing standards ISO 9806:2017 [20]. Likewise, the wind speed turbulence level for the 2.4 and 4.6 m/s wind speed was found to be 25.6% and 26.8%, respectively. These levels are within the ISO 9806:2017 [20] recommended range of 15% to 40% for simulating natural wind conditions.

During testing, both modules were electrically connected in series to an adjustable load to maintain their operation at maximum power point to ensure that the thermal characterization is obtained under realistic electrical operating conditions.

The identification of steady-state periods is done using the criteria listed in Table 5. According to ISO 9806:2017 [20], steady-state conditions should be determined by comparing the deviation of 30-s averages of certain parameters to their average value during the measurement period. In this experiment, measurement periods of 20 min are used.

Table 5. Steady-state criteria for indoor testing.

Parameter	Maximum Deviation (ISO 9806:2017 [20])	Maximum Deviation Used
Airflow rate $\dot{m}_o$	2%	2%
PV temperatures T_{A1-A11}, T_{B1-B11}	–	0.8 °C
Outlet temperature T_o	1.5 °C	0.25 °C
Inlet temperature T_i	1.5 °C	1.3 °C
Ambient temperature T_a	1.5 °C	0.6 °C
Net long-wave irradiance E_L	20 W/m^2	15 W/m^2
Irradiance G	50 W/m^2	Not applicable
Wind speed V_w	1.0 m/s deviation from set value	Not applicable

Table 5 contains the maximum deviation allowed for the different parameters to consider the collector in steady-state. The maximum deviation is the largest difference between any 30-s data within a 20-min measurement period and the mean value obtained during that period. The deviation for the irradiance and wind speed is given by the uniformity scans, as they are not logged during testing.

3.3. Outdoor Electrical and Thermal Characterization

The outdoor BIPVT thermal and electrical characterization was conducted on the rooftop of a building at Kongju National University in Cheonan, Korea. As shown in Figure 6, the experiment facility is comprised of a two-axis tracker (horizontal, vertical),

heating and cooling facilities (air chamber) to vary the inlet air temperature and a controller. The two-axis tracker adjusts position of the collector to maximize incident solar radiation. Inlet and outlet distribution boxes ensure the airflow uniformity within the collector. The installed sensors include a pyranometer, ambient temperature and humidity sensors as well as a wind direction and wind speed sensor, as shown in Table 6.

Figure 6. BIPVT collector outdoor experimental setup.

Table 6. Instrument specifications.

Measurement	Instrument Type	Instrument Accuracy
Ambient temperature T_a	Humidity and temperature transmitter	0.1 °C·T_a
Outlet temperature T_o		0.1 °C·T_o
Inlet temperature T_i		0.1 °C·T_i
Ambient relative humidity RH		0.8%·T_a
Air flowrate $\dot{m}_o$	Insertion mass flow meter	0.5%·$\dot{m}$
Wind speed V_w	Ultrasonic anemometer	0.1 m/s·V_w
Irradiance G	Pyranometer	1.2%·G
PV cell temperature T_{pv}	Thermocouple Type T	0.5%
Current I	I-V curve tracer	±1 mA
Voltage V	I-V curve tracer	±5 mV

The outdoor experiments were conducted from March to October 2021 with a single BIPVT collector unit installed in a closed-loop configuration (Figure 7). Temperature and humidity sensors as well as flowmeters were installed at both the collector inlet and outlet, while the PV module temperature were measured by 11 thermocouples mounted at the back of the absorber rear glass sheet. The BIPVT collector was connected to a MPPT I-V curve tracer to determine the thermal characteristics under realistic electrical operating conditions, i.e., when the PV operates at maximum power point—as described by ISO 9806:2017 [20]—while allowing electrical characteristics such as P_{mp}, V_{oc}, and I_{sc}, to be measured.

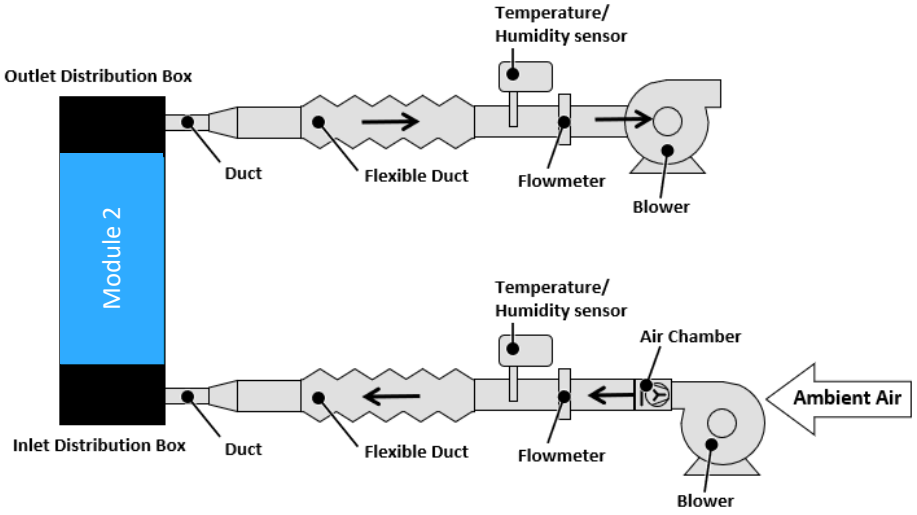

Figure 7. Outdoor experimental setup schematic.

Thermal performance was obtained based on ISO 9806:2017 [20] testing standards for solar thermal collectors. The system is considered under steady-state conditions when the inlet and outlet flowrate, inlet and outlet temperature and ambient temperature measurements are within the permitted deviation, shown in Table 5, for 10 min. ISO 9806:2017 [20] specifies a 20-min steady-state period; however, it is challenging to maintain steady-state outdoors for longer periods. Therefore, the steady-state period was shortened to 10 min. Table 7 presents the range of the different measurements used for the electrical and thermal performance assessment.

Table 7. Range of the different measurements during the outdoor steady-state experiment.

Parameters	Electrical Experimental Value Range	Thermal Experimental Value Range
Irradiance G	817–988 W/m^2	722–1015 W/m^2
Ambient temperature T_a	11–28 °C	11–31 °C
Outlet airflow rate $\dot{m}_o$	111–234 kg/h	113–234 kg/h
Inlet air temperature setpoint T_i	10, 15, 20, 25, 30 °C	15, 20, 25, 30 °C
Outlet temperature T_o	23–42 °C	36–40 °C
Wind speed V_w	0.5–1.8 m/s	0.9–1.9 m/s

4. Results and Discussion

4.1. Indoor Performance

4.1.1. Electrical Performance

The I-V curve measurements taken in the LAPSS under different module temperatures and irradiance conditions are used to perform the electrical characterization and determine the temperature coefficients for open-circuit voltage and maximum power point.

According to IEC 60891 Ed.2 [21], the open-circuit voltage temperature coefficient β corresponds to the slope of the open-circuit voltage V_{oc} as a function of the module temperature T_{pv}. The open-circuit voltage as a function of the module temperature is plotted in Figure 8 for different irradiance levels. The relative β is −0.26%/°C, corresponding to the slope of the curve at 1000 W/m^2 and a V_{oc} at 25 °C.

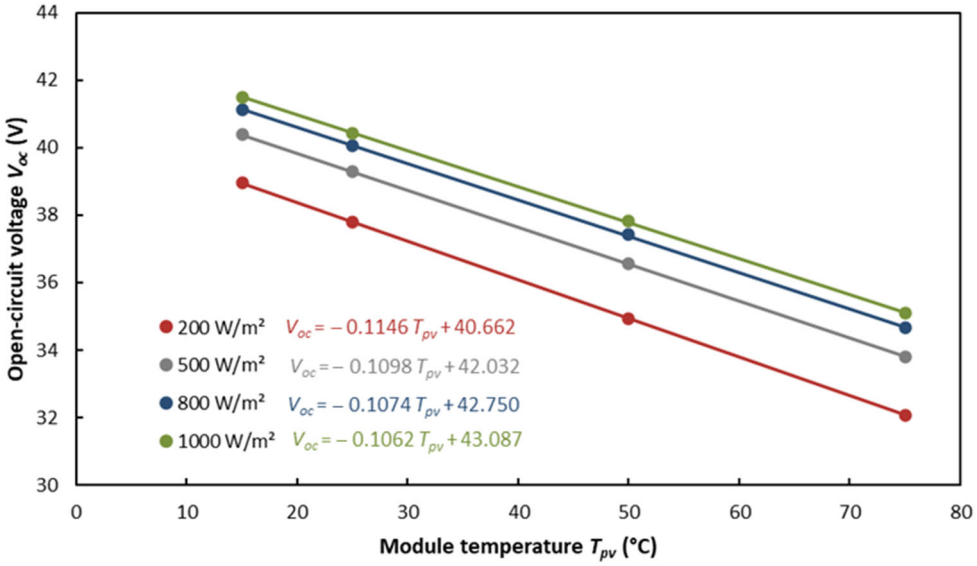

Figure 8. Open-circuit voltage dependence to module temperature at various irradiance levels.

The maximum power point temperature coefficient γ corresponds to the slope of the maximum power point P_{mp} as a function of the module temperature T_{pv}. Figure 9 illustrates how the maximum power decreases as the module temperature increases and irradiance decreases. The relative γ for the curve at 1000 W/m^2 is $-0.36\%/°C$.

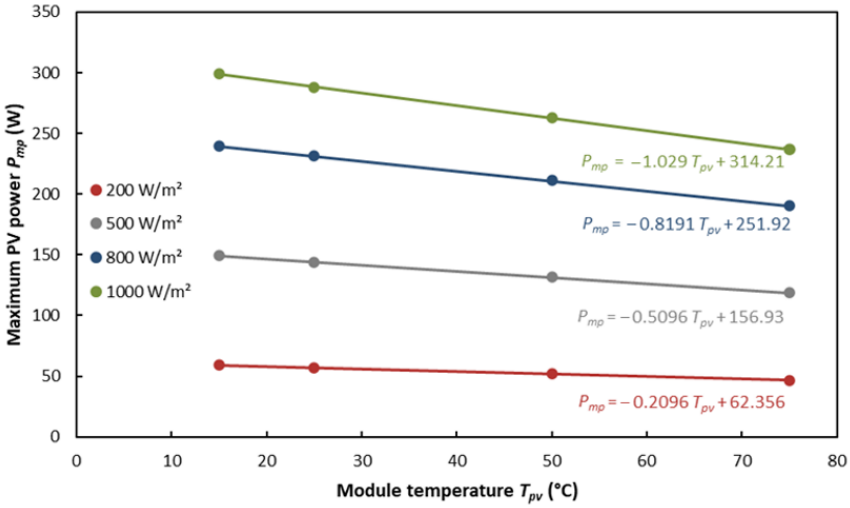

Figure 9. Maximum power dependence to module temperature at various irradiance levels.

4.1.2. Thermal Performance

Multiple indicators, such as the air temperature rise T_{rise} across the collector, characterize the thermal performance of a BIPVT collector. It is given by:

$$T_{rise} = T_o - T_i \quad (1)$$

In Equation (1), T_i and T_o are the air inlet and outlet air temperature (°C), respectively. T_o is given by the RTD measurement located downstream of the outlet distribution box. In the open-loop configuration, T_i corresponds to the average of the three inlet thermocouples and is typically very close to ambient. In the closed-loop configuration, T_i corresponds to the RTD measurement located upstream of the inlet distribution box.

The collector thermal output Q_{th} (W) is obtained using Equation (2), where $\dot{m}_o$ is the collector airflow rate measured downstream of the collector (kg/h), assuming no

air infiltration between the collector inlet and the flowmeter, and h_i and h_o are the air specific enthalpy at the inlet and outlet (J/kg) calculated using the ASHRAE Fundamentals Handbook [24] equations for moist air. The thermal efficiency η_{th} (%) is calculated with Equation (3), where G'' is the net solar irradiance and A_g is the gross area of both modules (i.e., 3.49 m^2).

$$Q_{th} = \dot{m}_o(h_o - h_i) * \frac{1\ h}{3600\ s} \tag{2}$$

$$\eta_{th} = \frac{Q_{th}}{G'' A_g} * 100 \tag{3}$$

For unglazed collectors, the net solar irradiance G'' (W/m^2) is calculated using Equation (4), where E_L is the net long-wave irradiance (W/m^2) measured by the pyrgeometer, σ is the Stefan-Boltzmann constant ($W/(m^2 \cdot K^4)$), T_a is the ambient temperature (°C) and ε/α is the collector emissivity over absorptance ratio. This value is set to 0.85, as recommended in ISO 9806:2013 [19].

$$G'' = G + \frac{\varepsilon}{\alpha}(E_L - \sigma(T_a + 273.15)^4) \tag{4}$$

The reduced temperature T_m^* ($m^2 \cdot K/W$) is calculated using Equation (5).

$$T_m^* = \frac{\left(\frac{T_o + T_i}{2}\right) - T_a}{G''} \tag{5}$$

The thermal efficiency as a function of airflow rate for an irradiance of 939 W/m^2 in open-loop configuration is shown in Figure 10. The total uncertainty associated with each measurement includes the accuracy of both the instruments and data acquisition system, details for the uncertainty calculations are provided in Appendix A. As expected, the thermal efficiency increases with airflow rate due to the increased amount of heat transfer occurring inside the collector. However, it decreases with wind speed, since higher wind speeds increase the heat losses from the absorber to the environment. At a medium irradiance level of 939 W/m^2 and wind speed of 2.4 m/s, the thermal efficiency increases from 18% to 42% when the flowrate changes from 85 to 350 kg/h.

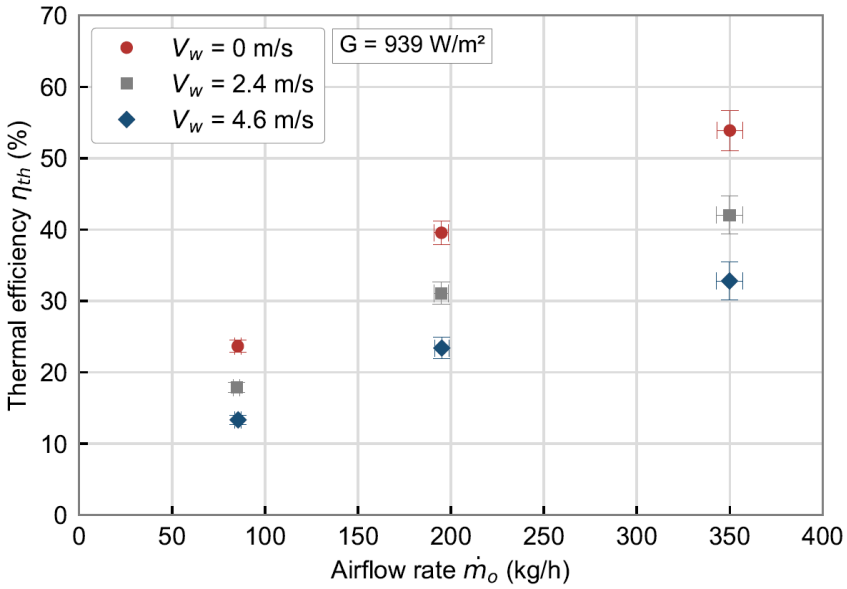

Figure 10. Thermal efficiency dependency to flowrate and wind speed.

Furthermore, the temperature rise across the collector decreases as the airflow rate and wind speed increase, as seen in Figure 11, but increases at higher irradiance levels

(Figure 12). Under still air condition and medium irradiance level of 939 W/m^2, the temperature rise is reduced by 15 °C when the flowrate changes from 85 to 350 kg/h.

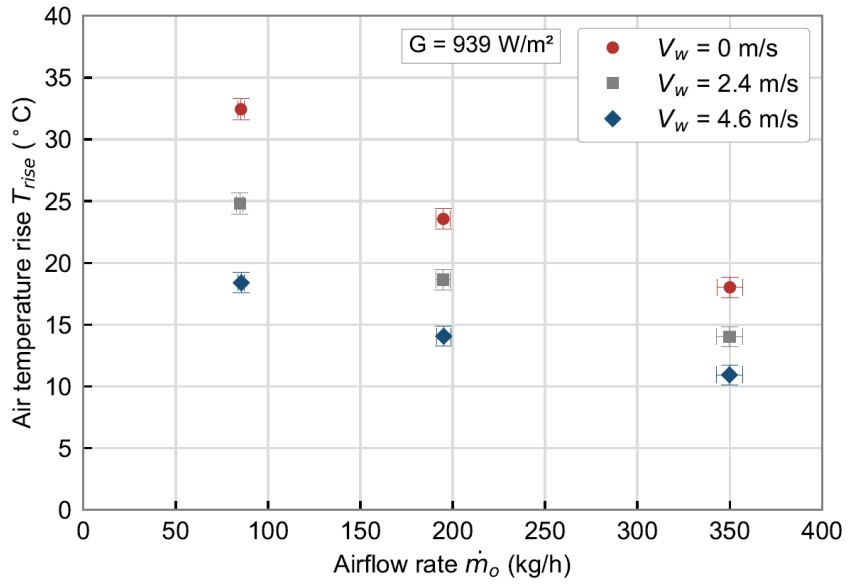

Figure 11. Temperature rise dependency to flowrate and wind speed.

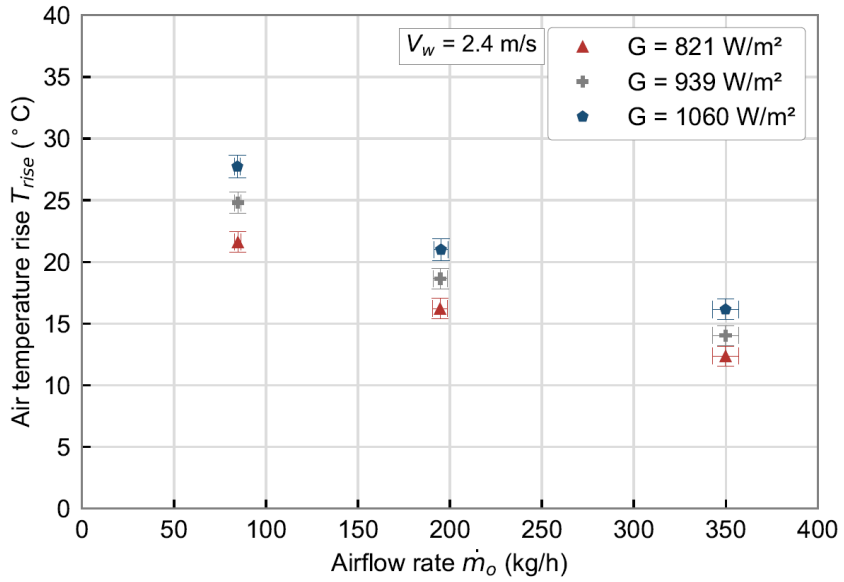

Figure 12. Temperature rise dependency to flowrate and irradiance.

As described in ISO 9806:2017 [20], the thermal efficiency can also be represented as a function of the reduced temperature difference T_m^* for a closed-loop configuration. Figure 13 shows the thermal efficiency for all testing conditions as a function of T_m^* for both open-loop (points in the red left portion of the graph) and closed-loop (points in the white right portion of the graph) configurations. Typically, open-loop results are not represented as a function of the reduced temperature difference. However, due to the dual open- and closed-loop operation, T_m^* is used to compare the overall performance. As expected, increasing the reduced temperature difference decreases the thermal efficiency drastically.

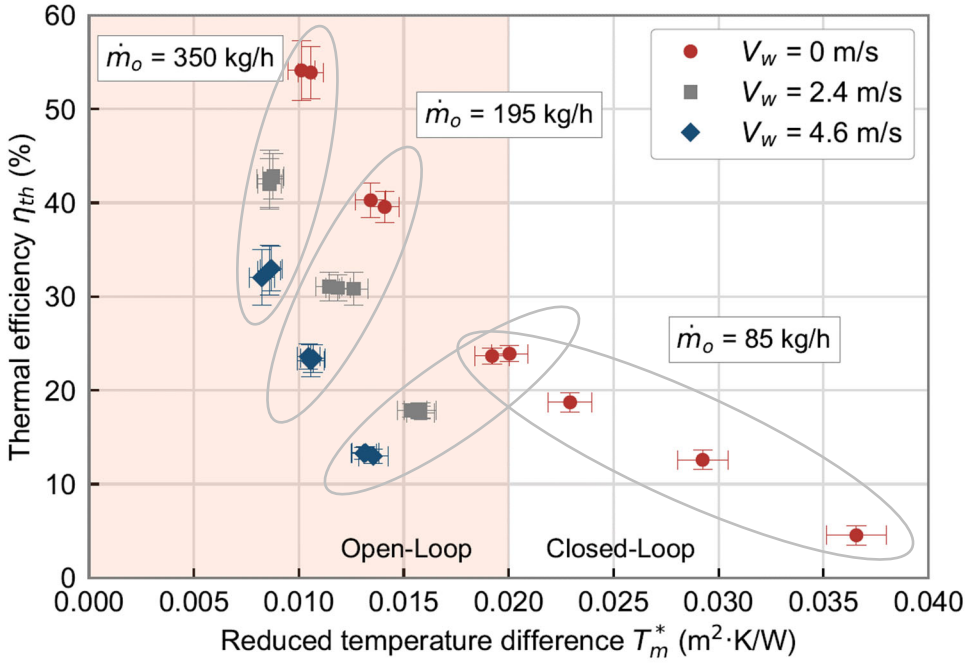

Figure 13. Thermal efficiency for all testing conditions for both open- and closed-loop at different reduced temperatures.

4.2. Outdoor Performance

4.2.1. Electrical Performance

The open-circuit voltage V_{oc} as a function of the module temperature T_{pv} is plotted in Figure 14 at different irradiance levels. The relative open-circuit voltage temperature coefficient β is $-0.27\%/^{\circ}C$ above 930 W/m^2.

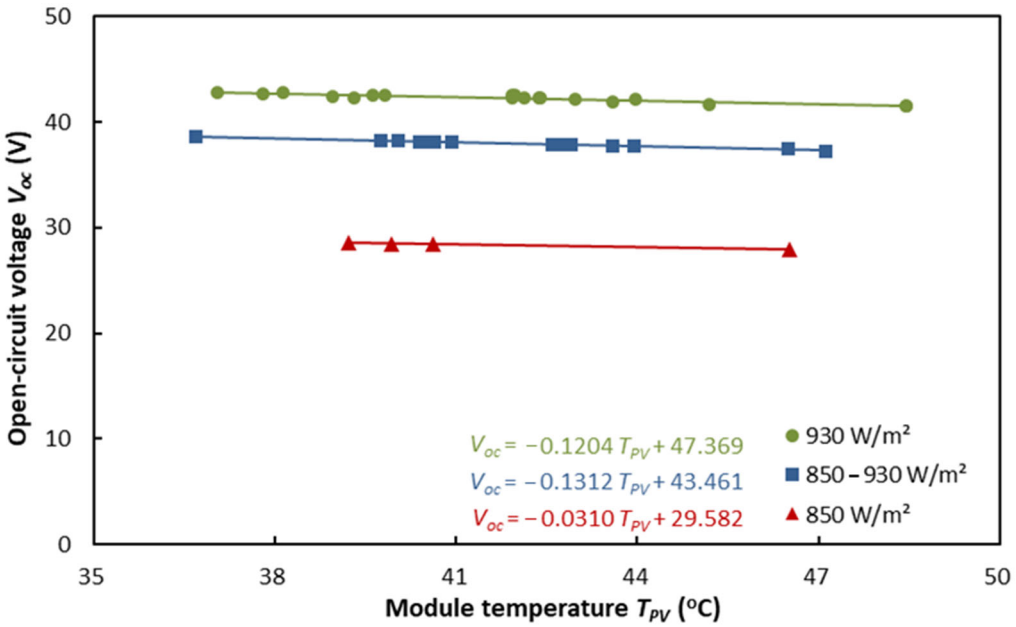

Figure 14. Outdoor open-circuit voltage as a function of module temperature under various irradiance levels.

Figure 15 illustrates that P_{mp} decreases as T_{pv} increases and irradiance decreases. The relative maximum power point temperature coefficient γ above 930 W/m^2 is $-0.53\%/^{\circ}C$.

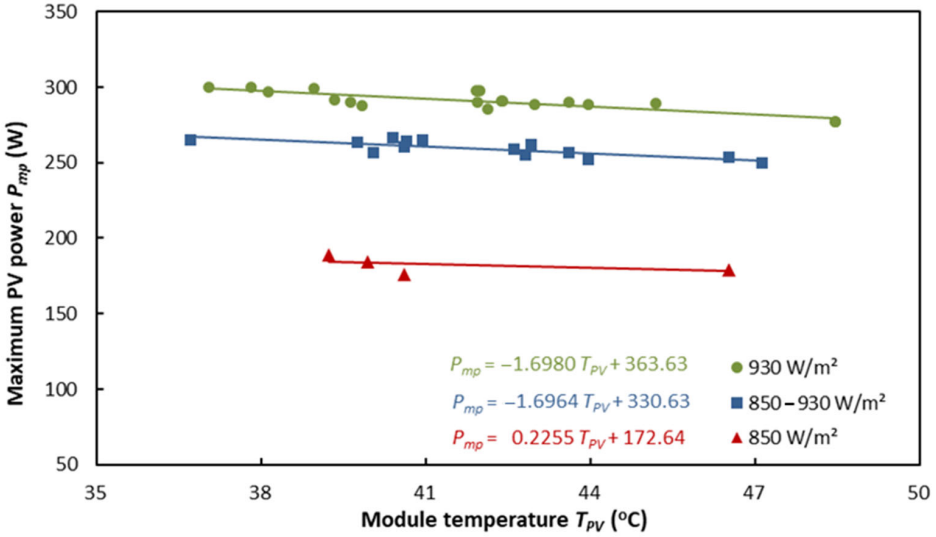

Figure 15. Outdoor maximum power as a function of module temperature under various irradiance levels.

4.2.2. Thermal Performance

The thermal efficiency, used to assess the BIPVT thermal performance, was calculated in accordance with ISO 9806:2017 [20] and is given by Equation (3). For the outdoor tests, the collector thermal output is given by Equation (6).

$$\dot{Q}_{th} = \left(\left(\dot{m}_o C_{f,o} T_o\right) - \left(\dot{m}_i C_{f,i} T_i\right) - \left[\left(\dot{m}_o - \dot{m}_i\right) C_{f,a} T_a\right]\right) * \left(\frac{1\ h}{3600\ s}\right) \quad (6)$$

where $C_{f,o}$ is the outlet specific heat of air at a constant pressure (J/(kg·°C)), $\dot{m}_i$ is inlet flow rate upstream of the collector (kg/h), $C_{f,i}$ is the inlet specific heat of air at a constant pressure (J/(kg·°C)), $C_{f,a}$ is the outdoor specific heat of air at a constant pressure (J/(kg·°C)).

Figure 16 shows the thermal efficiency as a function of reduced temperature difference T_m^*, ambient temperature and irradiance. The reduced temperature difference is calculated with the net irradiance G''. However, since the net long-wave irradiance is not measured in the outdoor experiment, a constant value of -100 W/m^2 is used as suggested in ISO 9860:2017 [20] for a clear sky day. As expected, the thermal efficiency decreases with increasing reduced temperature difference. It ranges between 12% and 39%.

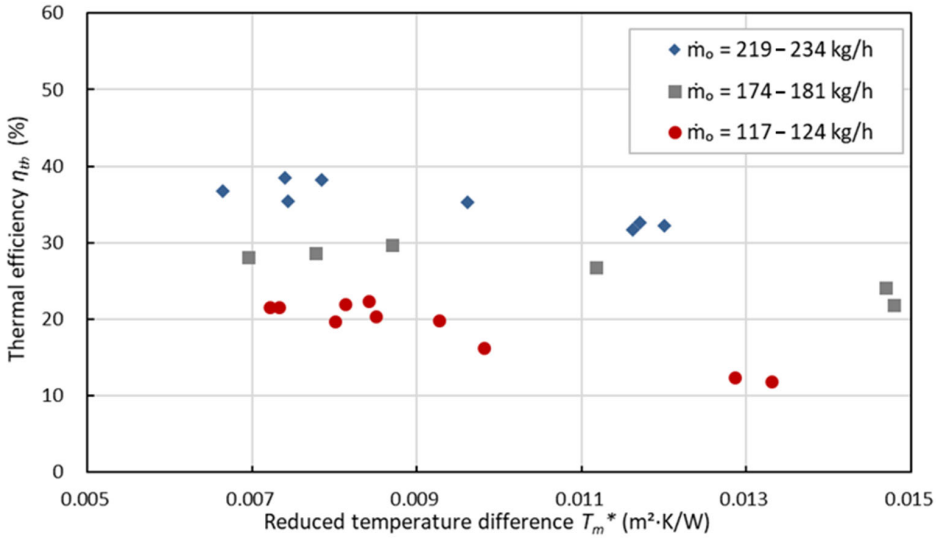

Figure 16. Thermal efficiency at different reduced temperatures and flow rates.

4.3. Indoor and Outdoor Experiment Comparison

4.3.1. Comparison Challenges

The literature review presented in Section 1 demonstrated the incomparability of the experimental results provided in the literature to the current study as different experimental conditions, standards and collector designs were used. However, there are also challenges when comparing a similar BIPVT design with the same standards, such as the results obtained with the indoor and outdoor experiments. These challenges are due to differences in:

- Environmental testing conditions
- BIPVT collector area
- Experimental setup.

These challenges are not specific to BIPVT air collectors as they also apply to air solar thermal collectors, BIPV modules or standard photovoltaic modules with thermal energy recovery (PVT). This highlights, however, that BIPVT air collector testing requires several considerations as it combines the particularities of different solar thermal technologies.

Environmental Testing Conditions

The level of solar irradiance control in an outdoor environment is limited. A two-axis tracking system can provide some level of control, but it is limited to the available global solar radiation. In addition, depending on the testing site, the level of ground reflected radiation can change significantly throughout the day with a two-axis tracking system which can make it difficult to reach steady-state conditions. In outdoor conditions, however, solar irradiance uniformity is much easier to achieve than in an indoor solar simulator.

Reliable and representative wind speed measurements are difficult to obtain in both indoor and outdoor conditions. Consequently, a direct comparison of indoor and outdoor wind speed measurements should also be done with care. In this study, the indoor tests use a wind generator located close to the collector inlet whereas the outdoor tests rely solely on natural wind. The uniformity provided by the indoor wind speed generator degrades along the length of the BIPVT collectors, whereas the outdoor setup may provide a better uniformity. Conversely, the two-axis tracking system used during the outdoor testing might affect the wind direction on the collector and, consequently, the convective heat losses at the surface of the absorber.

BIPVT Collector Area

The indoor experiment involved two collectors in series whereas the outdoor test used only one unit. In addition, the collector used for the outdoor test had a slightly greater length than the individual units of the indoor experiments. Thus, length-dependent measurements such as temperature rise and average PV temperature cannot be used for comparison as the results would differ significantly with increasing length. In addition, the impact of the entrance region might have been greater in the outdoor experiment than during the indoor tests.

Experimental Setup

The collector airflow uniformity has an important impact on the heat transfer inside the channel and, consequently, on the unit thermal performance. Distribution boxes were used in both experiments to promote flow uniformity in the channel, but with different designs. ISO 9806:2017 [20] does not specify a method to validate the flow uniformity; therefore, it was not verified, and this can affect the comparability of the results.

The air solar thermal and BIPVT slope also has an impact on the heat transfer inside the channel as it affects the level of natural convection, especially at lower flowrates, and potentially the flow uniformity. The indoor thermal characterization was conducted in a vertical (open-loop tests) and horizontal (closed-loop tests) orientation, while the outdoor experiment utilized a two-axis tracking system that varied the slope of the unit.

Consequently, variations in the slope might be a source of discrepancies between the indoor and outdoor experimental measurements.

In ISO 9806:2017 [20], it is required that PVT collectors be operated at maximum power point (MPP) during thermal testing. Thus, I-V curves must be traced frequently to ensure that maximum power point is maintained. Tracing I-V curves, even if completed quickly, influences the collector thermal performance and can lead to the loss of steady-state conditions. This is an important issue when conducting outdoor testing.

Finally, BIPVT collectors bring an additional challenge during testing in comparison with PVT collectors as they are meant to be building-integrated. The collector under study already had insulation at the back surface, but when it is not the case, an appropriate level of insulation might need to be considered to replicate real operating conditions.

4.3.2. Results

A comparison of the indoor and outdoor electrical performance obtained is presented in Table 8. Note that the indoor power and efficiency values presented are not actual measurements, but interpolated values to match the PV module temperature and irradiance conditions obtained outdoors. Under similar conditions, the indoor and outdoor module power deviated by 10% due to a different number of cells for each module, while the outdoor electrical efficiency was slightly lower than that obtained indoors. These differences could be attributed to environmental testing conditions, but they could also be due to variations introduced during manufacturing, despite utilizing BIPVT collectors of identical designs.

Table 8. Indoor and outdoor electrical characterization comparison.

Parameters	Indoor Experiment	Outdoor Experiment
Irradiance (G)	967 W/m^2	967 W/m^2
Maximum power (P_{mp})	259 W *	289 W
PV module temperature (T_{pv})	45 °C	45 °C
Electrical Efficiency (η_{pv})	15.3% *	14.2%
Open-circuit voltage temperature coefficient (β)	−0.26%/°C	−0.27%/°C
Maximum power point temperature coefficient (γ)	−0.36%/°C	−0.53%/°C

* Indoor power and efficiency values are interpolated to correspond to the outdoor G and T_{pv}.

Considering the challenges mentioned in Section 4.3.1, a limited number of variables can be used to compare the indoor and outdoor thermal characterization. As such, the thermal efficiency is the sole comparable metric as it is not dependent on the BIPVT area. Therefore, the indoor and outdoor thermal efficiency as a function of airflow rate is compared in Figure 17 under similar wind velocities and inlet reduced temperature difference T_i^*. The results were filtered to a T_i^* below 0.003 m^2·K/W to compare the results under similar reduced temperatures. Since the indoor test used two units in series with a similar width of the module tested outdoors, both setups had similar inlet cross-sectional areas. As a result, the airflow rate is used as an independent variable in this figure to ensure a fair comparison between the two experiments. The inlet reduced temperature difference is calculated as a function of the air inlet temperature, ambient temperature and long-wave irradiance, as shown in Equation (7). In this case, it is preferred to T_m^*, presented in Section 3 to avoid using the air outlet temperature, a length-dependent variable.

$$T_i^* = \frac{T_i - T_a}{G''} \tag{7}$$

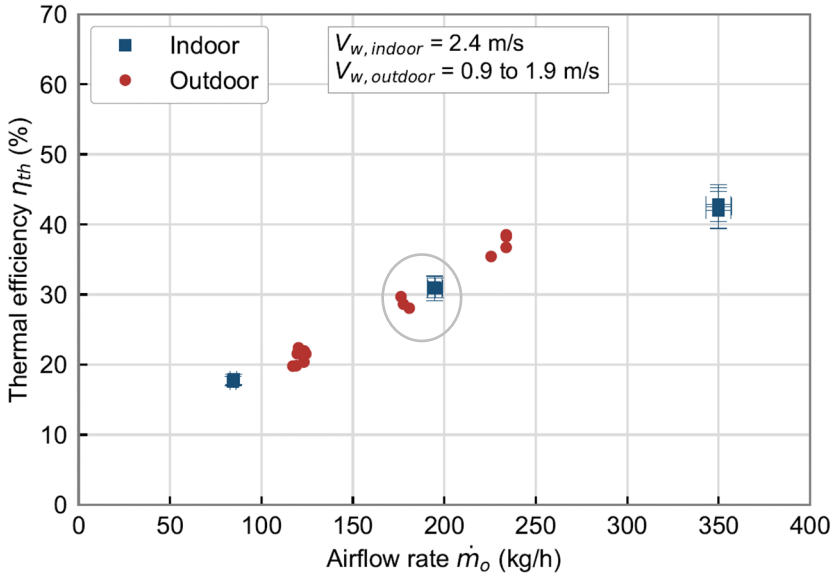

Figure 17. Indoor and outdoor thermal efficiency comparison as a function of specific airflow rate with $T_i^* < 0.003$ m^2·K/W.

Figure 17 illustrates that the indoor and outdoor thermal efficiency follows a similar trend for $T_i^* < 0.003$ m^2·K/W under comparable wind speed conditions. The outdoor experimental deviations are due to the differences in wind speed, ambient temperature and irradiance. These parameters varied throughout the outdoor experiment, despite being sufficiently stable to be considered under steady-state conditions. Table 9 compares the indoor and outdoor thermal efficiency under similar, yet not identical, conditions. It shows that the indoor thermal efficiency is 31.1% and 28.6% for an airflow rate of 195 kg/h and 174 kg/h for the indoor and outdoor results, respectively.

Table 9. Indoor and outdoor thermal performance characterization comparison.

Parameters	Indoor Experiment	Outdoor Experiment
Gross BIPVT area (A_g)	3.49 m^2	2.11 m^2
Irradiance (G)	939 W/m^2	946 W/m^2
Wind speed (V_w)	2.4 m/s	0.9–1.9 m/s
Outlet airflow rate ($\dot{m}_o$)	195 kg/h	174 kg/h
Thermal efficiency (η_{th})	31.1%	28.6%
Inlet reduced temperature (T_i^*)	0.0016 m^2·K/W	0.0009 m^2·K/W

4.4. BIPVT Thermal Enhancement Comparison

This section compares the indoor experimental performance of two BIPVT collectors uniquely designed to enhance thermal performance. Both collectors were tested at Concordia University's SSEC with similar indoor testing conditions and configurations. Design A is a BIPVT unit with a hybrid PV/thermal absorber consisting of alternating rows of PV cells and curved solar thermal absorbers (Figure 18) [25]. Design B is the unit studied in Sections 1–3 and 4.1–4.3, i.e., a BIPVT collector with an absorber that consists solely of PV cells with an in-channel perforated baffle plate, as described in Section 2. A comparison between both collectors is shown in Table 10.

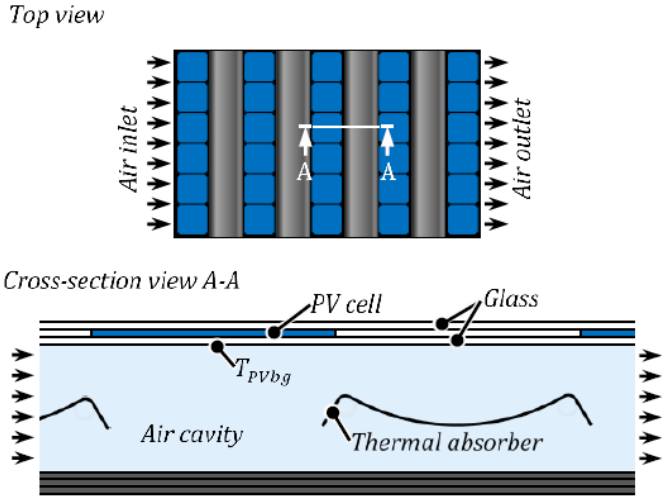

Figure 18. Design A cross-sectional view [18].

Table 10. Collector A and B characteristics.

Parameters	Design A	Design B
Gross area for 2 units (A_g)	3.27 m^2	3.49 m^2
Number of cells	30	60
Maximum power (P_{mp}) [1]	120.3 ± 2.5 W	287.8 ± 3.6 W
Electrical efficiency (η_{pv}) [1]	7.8 ± 0.2%	17.7 ± 0.2%

[1] At Standard Testing Conditions (STC).

The comparison of the two collectors is done using the outlet specific airflow rate $\dot{m}_{o,s}$ (kg/(h·m^2)) calculated with Equation (8).

$$\dot{m}_{o,s} = \frac{\dot{m}_o}{A_g} \tag{8}$$

The electrical efficiency η_{pv} (%) is calculated using Equation (9).

$$\eta_{pv} = \frac{P_{mp}}{GA_g} * 100 \tag{9}$$

Figures 19–21 show the thermal and electrical performance under still air conditions (V_w = 0 m/s) and low irradiance levels for both collectors while Table 11 shows a comparison of the two designs at similar conditions. Design B's electrical efficiency is 2.3 times greater due to the added PV cells on the absorber compared to Design A. However, the thermal efficiency of Design A is, on average, 1.2 times greater than Design B. At low flowrate, Design A also has a thermal and electrical efficiency of 25.1% and 5.9%, respectively. Under similar conditions, Design B has a thermal efficiency of 23.9% and an electrical efficiency of 13.5%. This means that under these conditions, a BIPVT collector with a standard PV module as an absorber and an in-channel perforated baffle plate can substantially increase the electrical efficiency with a slight decrease in the thermal efficiency compared to a BIPVT collector with a hybrid PV/thermal absorber.

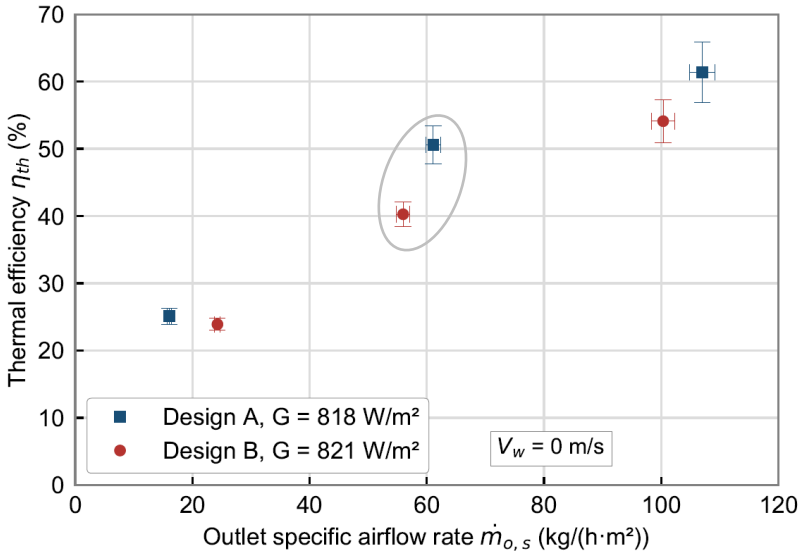

Figure 19. Thermal efficiency comparison as a function of the outlet specific airflow rate.

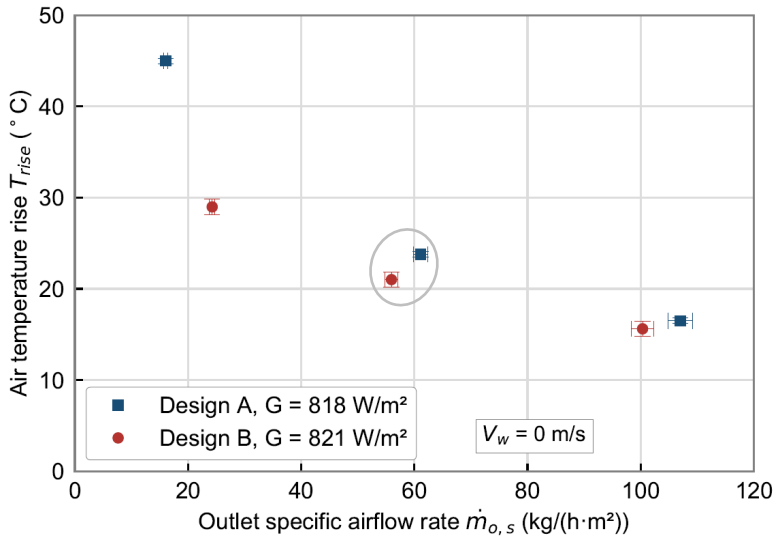

Figure 20. Temperature rise comparison as a function of the outlet specific airflow rate.

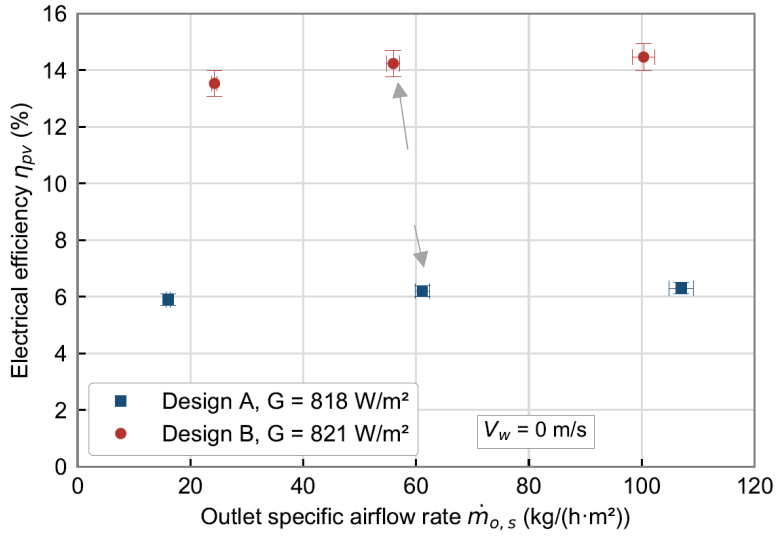

Figure 21. Electrical efficiency comparison as a function of the outlet specific airflow rate.

Table 11. Design A and B thermal performance characterization comparison.

Parameters	Design A	Design B
Outlet specific airflow rate ($\dot{m}_{o,s}$)	107 kg/(h·m^2)	100 kg/(h·m^2)
Irradiance (G)	818 W/m^2	821 W/m^2
Wind speed (V_w)	0 m/s	0 m/s
Air temperature rise (T_{rise})	16.2 °C	15.6 °C
Thermal efficiency (η_{th})	60.3%	53.9%
Electrical efficiency (η_{th})	6.4%	14.1%
Maximum power (P_{mp})	170.7 W	403.8 W

In summary, for a similar sized system, utilizing a 100% PV module yields a similar thermal performance compared to a BIPVT module with 50% PV cells and 50% solar thermal absorbers that was specially designed for a higher thermal output. Thus, designs that benefit from higher electrical generation and a moderately high thermal output should consider the use of a thermal enhanced BIPVT module with 100% PV cells as opposed to a hybrid PV/thermal absorber.

5. Conclusions

This study presented the results of indoor and outdoor experiments to assess the thermal and electrical performance of an air-type BIPVT collector with an in-channel perforated baffle plate. It also provided a comparison to a BIPVT unit with a hybrid PV/thermal absorber consisting of alternating rows of PV cells and curved solar thermal absorbers.

The indoor experiments were conducted in a Large Area Pulse Solar Simulator as well as at the Concordia University Paul Fazio Solar Simulator and Environmental Chamber (SSEC) located in Montreal, Canada. Electrical and thermal properties were assessed according to IEC 60904-9 [23] and ISO 9806:2017 [20], respectively. The outdoor experiments were conducted at Kongju National University, and the thermal and electrical performance was evaluated according to ISO 9806:2017 [20].

The indoor thermal characterization was conducted in both open-loop and closed-loop conditions. Under open-loop conditions, a thermal efficiency between 18% and 42% was obtained corresponding to a temperature rise between 12 and 28 °C when varying the airflow rate from 85 to 350 kg/h at an average wind speed of 2.4 m/s.

Under closed-loop conditions, the outdoor measurements provided thermal efficiencies between 12% and 39% with a flowrate varying between 117 and 234 kg/h, a wind speed in the range of 0.9 to 1.9 m/s and an irradiance from 722 to 1015 W/m^2.

Comparing indoor and outdoor experimental results proved challenging due to differences in environmental testing conditions (e.g., wind and solar uniformity), BIPVT collector area and experimental setup (e.g., flow uniformity and collector slope). These challenges are not specific to BIPVT air collectors as they also apply to air solar thermal collectors, BIPV modules, or standard photovoltaic modules with thermal energy recovery (PVT). In addition, as the standards are specific to PVT systems, when adhering to these testing standards for BIPVT systems, the results of the experiments could differ when the modules are integrated into a building. This highlights that BIPVT air collector testing requires several considerations as it combines the particularities of many solar thermal technologies. Such particularities should be considered in future standards for performance characterization.

Despite limited comparable points, the indoor and outdoor results provided similar thermal efficiencies that followed the same trend with respect to airflow rate. When comparing the performance of the BIPVT collector studied (Design B) to a BIPVT unit with a hybrid PV/thermal absorber consisting of alternating rows of PV cells and curved solar thermal absorbers (Design A), the electrical efficiency of Design B was found to be 2.3 times greater. However, the thermal efficiency was, on average, 1.2 times greater for Design A. This shows that a BIPVT collector with a standard PV module as an absorber

and an in-channel perforated baffle plate can substantially increase the electrical efficiency with a slight decrease in thermal efficiency compared to a BIPVT collector with a hybrid PV/thermal absorber.

Overall, the novelty of the study resides in the advancement of characterization testing methods for air-based BIPVT collectors since it demonstrated how existing PV and solar thermal standards can be used for thermal and electrical performance characterization and highlighted key considerations to include in future standard development. It also includes the demonstration of the added value of a new BIPVT collector design achieving a similar thermal performance than a module with a hybrid PV/thermal absorber, but without any loss in electrical performance.

Author Contributions: Conceptualization, J.-H.K., B.R., E.G.-L., V.D. and J.-T.K.; methodology, J.-H.K., B.R. and E.G.-L.; formal analysis, J.-H.K., J.-S.Y., B.R. and E.G.-L.; investigation, J.-S.Y., B.R. and E.G.-L.; resources, B.R., E.G.-L. and V.D.; data curation, J.-S.Y. and B.R.; writing—original draft preparation, J.-H.K., J.-S.Y., B.R., E.G.-L. and V.D.; writing—review and editing, J.-H.K., B.R., E.G.-L., V.D. and J.-T.K.; visualization, J.-S.Y., B.R. and E.G.-L.; supervision, V.D. and J.-T.K.; project administration, J.-H.K. and V.D.; funding acquisition, J.-T.K. All authors have read and agreed to the published version of the manuscript.

Funding: This research was funded by the Korea Institute of Energy Technology Evaluation and Planning (KETEP) and the Ministry of Trade, Industry and Energy (MOTIE) of the Republic of Korea, grant number 20188550000480.

Institutional Review Board Statement: Not applicable.

Informed Consent Statement: Not applicable.

Data Availability Statement: Not applicable.

Conflicts of Interest: The authors declare no conflict of interest.

Appendix A

The uncertainty utilized in the paper is provided and calculated from the manufacturer's specifications or calibration certificates, shown in Tables 3 and 6, and are known as Type B uncertainties. The standard uncertainty, u_B, will vary with the type of estimate. A detailed explanation of its calculation can be found in [26]. For a value calculated using a function f, the combined uncertainty, u_c, can be calculated using Equation (A1) assuming the estimates are independent.

$$u_c = \sqrt{\sum_{i=1}^{n} \left(\frac{\partial f}{\partial y_i}\right)^2 u^2 y_i} \quad \text{(A1)}$$

The calculated uncertainty assumes a coverage factor of 2 (for a 95% level of confidence) as it is not specified by the manufacturer. The expanded uncertainty calculated is used to compute the error bars in the figures.

References

1. Chaibi, Y.; Malvoni, M.; El Rhafiki, T.; Kousksou, T.; Zeraiuli, Y. Artificial neural-network based model to forecast the electrical and thermal efficiencies of PVT air collector systems. *Clean. Eng. Technol.* **2021**, *4*, 100132. [CrossRef]
2. University College London (UCL). *2020 Global Status Report for Buildings and Construction*; United Nations Environment Programme: Nairobi, Kenya, 2020; p. 10.
3. IEA PVPS. Trends in photovoltaic applications 2019. In *Task 1 Strategic PV Analysis and Outreach*; IEA PVPS: Rheine, Germany, 2019.
4. Kumar, S.P.; Agyekum, E.B.; Velkin, V.I.; Yaqoob, S.J.; Adebayo, T.S. Thermal management of solar photovoltaic module to enhance output performance: An experimental passive cooling approach using discontinuous aluminum heat sink. *Int. J. Renew. Energy Res.* **2021**, *11*, 1700–1712.
5. Agyekum, E.B.; Kumar, S.P.; Alwan, N.T.; Velkin, V.I.; Adebayo, T.S. Experimental study on performance enhancement of a photovoltaic module using a combination of phase change material and aluminum fins-Exergy, energy and economic (3E) analysis. *Inventions* **2021**, *6*, 69. [CrossRef]

6. Agyekum, E.B.; Kumar, S.P.; Alwan, N.T.; Velkin, V.I.; Shcheklein, S.E.; Yaqoob, S.J. Experimental investigation of the effect of a combination of active and passive cooling mechanism on the thermal characteristics and efficiency of solar PV module. *Inventions* **2021**, *6*, 63. [CrossRef]
7. Zondag, A.H.; De Vries, W.D.; Van Helden, W.G.J.; van Zolingen, R.J.C.; van Steenhoven, A.A. The yield of different combined pv-thermal collector designs. *Sol. Energy* **2003**, *74*, 253–269. [CrossRef]
8. De Vries, D.W. *Design of a Photovoltaic/Thermal Combi-Panel*; Technische Universiteit Eindhoven: Eindhoven, The Netherlands, 1998.
9. Adeli, M.M.; Sobhnamayan, F.; Farahat, S.; Alavi, M.A. Experimental performance evaluation of a photovoltaic thermal (PV/T) air collector and its optimization. *J. Mech. Eng.* **2012**, *58*, 309–318. [CrossRef]
10. Rahim, N.A.; Rahim, N.A.A.; Selvaraj, J.; Tyagi, V.V. Outdoor performance of solar PV/T air system. In Proceedings of the 2013 IEEE Conference on Clean Energy and Technology (CEAT), Langkawi, Malaysia, 18–20 November 2013; pp. 192–197.
11. Tomar, V.; Tiwari, G.N.; Bhatti, T.S. Performance of different photovoltaic-thermal (PVT) configurations integrated on prototype test cells: An experimental approach. *Energy Convers. Manag.* **2017**, *154*, 394–419. [CrossRef]
12. Ozakin, A.N.; Kaya, F. Experimental thermodynamic analysis of air-type PVT system using fins in different materials: Optimization of control parameters by Taguchi method and ANOVA. *Sol. Energy* **2020**, *197*, 199–211. [CrossRef]
13. Ciftci, E.; Khanlari, A.; Sozen, A.; Aytac, I.; Tuncer, A.D. Energy and exergy analysis of a photovoltaic thermal (PVT) system used in solar dryer: A numerical and experimental investigation. *Renew. Energy* **2021**, *180*, 410–423. [CrossRef]
14. Mojumder, J.C.; Chong, W.T.; Ong, H.C.; Leong, K.Y.; Mamoon, A.A. An experimental investigation on performance analysis of air type photovoltaic thermal collector system integrated with cooling fin design. *Energy Build.* **2016**, *130*, 272–285. [CrossRef]
15. Yang, T.; Athienitis, A.K. Experimental investigation of a two-inlet air-type building integrated photovoltaic/thermal (BIPV/T) system. *Appl. Energy* **2015**, *159*, 70–79. [CrossRef]
16. Cremers, J.; Mitina, I.; Palla, N.; Klotz, F.; Jobard, X.; Eicker, U. Experimental analyses of different PVT collector designs for heating and cooling applications in buildings. *Energy Procedia* **2015**, *78*, 1889–1894. [CrossRef]
17. Dittmann, S.; Friesen, T.; Frontini, F.; Bohren, A.; Zenhausern, D.; Rommel, M. Indoor and outdoor testing of an unglazed PVT collector. In Proceedings of the 29th European Photovoltaic Solar Energy Conference and Exhibition (EUPVSEC2014), Amsterdam, The Netherlands, 22–26 September 2014; pp. 3637–3640.
18. Bahtiar; Zohri, M.; Fudholi, A. Indoor and outdoor investigation comparison of photovoltaic thermal solar air collector. *Bull. Electr. Eng. Inform.* **2020**, *9*, 1311–1317. [CrossRef]
19. *ISO 9806:2013*; Solar Energy—Solar Thermal Collectors—Test Methods. International Organization for Standardization: Geneva, Switzerland, 2013.
20. *ISO 9806:2017*; Solar Energy—Solar Thermal Collectors—Test Methods. International Organization for Standardization: Geneva, Switzerland, 2017.
21. *IEC 60891 Ed.2:2009*; Photovoltaic Devices—Procedures for Temperature and Irradiance Corrections to Measured I–V Characteristics. International Electrotechnical Commission: Geneva, Switzerland, 2009.
22. Kim, J.H.; Yu, J.S.; Kim, J.T. An experimental study on the energy and exergy performance of an air-type PVT collector with perforated baffle. *Energies* **2021**, *14*, 2919. [CrossRef]
23. *IEC 60904-9:2020*; Photovoltaic Devices—Part 9: Classification of Solar Simulator Characteristics. International Organization for Standardization: Geneva, Switzerland, 2020.
24. ASHRAE. Chapter 6—Psychometrics. In *ASHRAE Fundamentals Handbook (SI)*; ASHRAE: Atlanta, GA, USA, 2001.
25. Delisle, V.; Kim, J.-T.; Kim, J.; Gagné, A.; Ayoub, J. *Performance Assessment of a New Air-Type Building-Integrated Photovoltaic Thermal Solar Collector*; EU PVSEC: Amsterdam, The Netherlands, 2017.
26. International Organization for Standardization. *Guide to the Expression of Uncertainty in Measurement*; International Organization for Standardization: Geneva, Switzerland, 1995; pp. 1–101.